

## A HIGH FALSE POSITIVE RATE FOR *KEPLER* PLANETARY CANDIDATES OF GIANT STARS USING ASTERODENSITY PROFILING <sup>†</sup>

David H. Sliski<sup>1,\*</sup> and David M. Kipping<sup>1,2</sup>

Draft version August 27, 2018

### ABSTRACT

Asterodensity Profiling (AP) is a relatively new technique for studying transit light curves. By comparing the mean stellar density derived from the transit light curve to that found through some independent method, AP provides information on several useful properties such as orbital eccentricity and blended light. We present an AP survey of 41 *Kepler* Objects of Interest (KOIs), with a single transiting candidate, for which the target star’s mean stellar density has been measured using asteroseismology. The ensemble distribution of the AP measurements for the 31 dwarf stars in our sample shows excellent agreement with the spread expected if the KOIs were genuine and have realistic eccentricities. In contrast, the same test for the 10 giants in our sample reveals significant incompatibility at  $> 4\sigma$  confidence. Whilst extreme eccentricities could be invoked, this hypothesis requires four of the KOIs to contact their host star at periastron passage, including the recently claimed confirmation of Kepler-91b. After carefully examining several hypotheses, we conclude that the most plausible explanation is that the transiting objects orbit a different star to that measured with asteroseismology - cases we define as false-positives. Based on the AP distribution, we estimate a false-positive rate (FPR) for *Kepler’s* giant stars with a single transiting object of  $FPR \simeq 70\% \pm 30\%$ .

*Subject headings:* Eclipses - methods: data analysis - planetary systems - planets and satellites:  
general techniques: photometric

### 1. INTRODUCTION

Over the last five years *Kepler* has revolutionized our understanding of exoplanetary systems with the discovery of several thousand planetary candidates<sup>5</sup>. One of the revelations to have emerged from this avalanche of objects is that conventional follow-up techniques for transit surveys, such as radial velocity observations, are impractical and prohibitively expensive when faced with several thousand targets. For this reason, great effort has been spent to find alternative methods to validate planetary systems which can ideally make use of the original *Kepler* data alone, such as blend analysis (Torres et al. 2011), Transit Timing Variations (TTV) (Nesvorný et al. 2012), planetary reflection/emission (Esteves et al. 2013) and validation by multiplicity (Lissauer et al. 2014; Rowe et al. 2014). With the upcoming TESS (Ricker et al. 2010) and PLATO (Rauer et al. 2013) missions expected to discover tens of thousands more planetary candidates, these techniques will be of great value to the wider community. In this vein, a new technique dubbed “Asterodensity Profiling” (AP) has recently been proposed as a tool to both aid in planetary validation and measuring the orbital eccentricity of planetary candidates (see Kipping et al. 2012a; Dawson & Johnson 2012; Kipping 2014a and references therein).

AP exploits the fact that one can infer the mean stellar density of a star,  $\rho_{\star, \text{obs}}$ , from the shape of a transit light curve under various idealized assumptions, as

first demonstrated by Seager & Mallen-Ornélas (2003). If one has some independent measure of the mean density,  $\rho_{\star, \text{true}}$ , a direct comparison allows one to test these idealized assumptions and ultimately extract useful information about the properties of the system. For example, Dawson & Johnson (2012) showed how the orbital eccentricity of a planet may be inferred using the so-called “photo-eccentric” effect and Kipping (2014a) showed how the quantity of blended light may be constrained using the “photo-blend” effect. Generally, cases where the two derived densities are dramatically different are the most interesting, since these immediately imply that the idealized assumptions cannot hold (Dawson et al. 2013).

The most accurate and precise independent measure of a star’s mean density comes from asteroseismology by measuring the large frequency spacing between the pulsation modes (Ulrich 1986). Thanks to *Kepler’s* precise and stable short cadence (SC) photometry (Gilliland et al. 2010), observers have derived fundamental properties for dozens of targets hosting planetary candidates (Huber et al. 2013). It is worth noting that since giants and sub-giant stars have greater pulsation amplitudes and timescales, *Kepler* targets with asteroseismology include considerably more low surface gravity stars than a random *Kepler* subset. This means that by using AP on this asteroseismology sample, we not only focus on the most well-characterized host stars, but we also have an opportunity to compare the ensemble population of planetary candidates associated with dwarfs versus giants.

In this work, we aim to demonstrate the value of AP in studying and characterizing transiting planetary candidates, where we limit our sample to only those stars with asteroseismically determined mean stellar densities. Since our sample contains a considerable number

<sup>1</sup> Harvard-Smithsonian Center for Astrophysics, 60 Garden St, Cambridge, MA 02138, USA

<sup>2</sup> Sagan Fellow

\* dsliski@cfa.harvard.edu

<sup>†</sup> Based on archival data of the *Kepler* telescope.

<sup>5</sup> See <http://archive.stsci.edu/kepler/planet.candidates.html>

of evolved host stars, we will also take this opportunity to use AP to compare the population of planetary candidates associated with dwarfs versus giants. Our analysis represents the first ensemble application of AP, although we note other authors have conducted ensemble analyses on *Kepler* candidates without using AP (e.g. Plavchan et al. 2014). In §2, we outline our sample and our methodology for conducting our survey using AP. In §3, we present the results of these efforts, including a comparison between the dwarf and giant population. In §4, we explore the possible value of AP for future missions and surveys as well as the implications of a high false-positive rate around giant stars.

## 2. METHODS

### 2.1. Sample Selection

From the several thousand *Kepler* Objects of Interest (KOIs) known at the time of writing, we focus on those KOIs with asteroseismically determined stellar densities. Whilst asteroseismology is not a requisite for conducting AP, it is usually the most accurate and precise measurement available and is often referred to as the “gold standard” (Bastien et al. 2013). Huber et al. (2013) recently provided a homogeneous catalog of asteroseismically determined stellar densities for 77 planet-candidate host stars. This sample, including 107 planetary candidates, forms the input catalog for our work. We subsequently refer to the independent measure of the stellar density used in our AP analysis as  $\rho_{\star, \text{astero}}$ .

In this work, we limit our sample to only those host stars with a single transiting planet candidate. The rationale for this choice is two-fold. First, one of the objectives of our work is to provide insights into the false-positive rate between the dwarf and giant planet-hosting stars and since multi-planet systems are known to have a very low false-positive rate (Lissauer et al. 2012, 2014), the single KOIs represent the more unknown subset. The second reason is that we propose that the single KOIs have a higher a-priori probability of exhibiting large AP discrepancies than the multiple planet systems. This choice can be understood by considering the six known AP effect discussed recently in Kipping (2014a):

- Photo-eccentric (PE) effect: Orbit of the transiting body is non-circular; causes  $\rho_{\star, \text{obs}} > \rho_{\star, \text{astero}}$  if  $0 < \omega < \pi$  and  $\rho_{\star, \text{obs}} < \rho_{\star, \text{astero}}$  if  $\pi < \omega < 2\pi$
- Photo-blend (PB) effect: A background, foreground or associated star dilutes the transit depth; causes  $\rho_{\star, \text{obs}} < \rho_{\star, \text{astero}}$
- Photo-timing (PT) effect: Unaccounted Transit Timing Variations (TTVs) affect the composite transit light curve; causes  $\rho_{\star, \text{obs}} < \rho_{\star, \text{astero}}$
- Photo-duration (PD) effect: Unaccounted Transit Duration Variations (TDVs) affect the composite transit light curve; causes  $\rho_{\star, \text{obs}} < \rho_{\star, \text{astero}}$
- Photo-spot (PS) effect: Unocculted starspots behave like an anti-blend, enhancing the transit depth; causes  $\rho_{\star, \text{obs}} > \rho_{\star, \text{astero}}$
- Photo-mass (PM) effect: The mass of the transiting body is significant and one cannot assume  $M_{\text{transiter}} \ll M_{\star}$ ; causes  $\rho_{\star, \text{obs}} > \rho_{\star, \text{astero}}$

Although we direct the reader to Kipping (2014a) for exact formulae and details of each AP effect, we point out that the PT, PD, PS and PM effects are all generally much weaker (typically  $\lesssim 10^{-1}$ - $10^0$  effect) than the PB and PE effects (typically  $\lesssim 10^1$ - $10^3$ ). Since large AP discrepancies are the most interesting to study, one should expect such variations to be caused by either the PB or PE effects. Multi-planet systems certainly have a low a-priori probability of exhibiting the PB effect, since the false-positive rate is known to be very low (Lissauer et al. 2012, 2014). They are also unlikely to have planets on large eccentricities in order to be dynamically stable, which means we expect low PE effects. For these reasons, we argue that single KOIs have a higher a-priori probability of exhibiting large and thus interesting AP discrepancies.

An added bonus of studying the single KOIs exclusively is that they are less probable, a-priori, to exhibit TTVs and thus the PT effect. Physically speaking, this is because they are less likely to have nearby planets near mean motion resonance inducing large perturbations (Agol et al. 2005; Holman et al. 2005). Mazeh et al. (2013) recently reported that multi-transiting KOIs exhibit significant TTVs in 120 out of 894 cases ( $\simeq 13\%$ ), whereas single-transiting KOIs show significant TTVs in just 23 out of 1066 cases ( $\simeq 2\%$ ). Since periodic TDVs are usually associated with periodic TTVs (Kipping 2009; Nesvorný et al. 2013), then the a-priori probability of the PD effect is also significantly less. On this basis, we argue that any large observed AP variations found in this sample are likely due to either i) the photo-eccentric effect, ii) the photo-blend effect or iii) the target with asteroseismology modes detected is not the same as the target with the transiting body.

In the Huber et al. (2013), there are 43 KOIs in single transiting systems. Of these, we exclude two objects for different reasons. KOI-42.01 shows strong TTVs (Van Eylen et al. 2013) and so falls in that small 2% category of dynamically active single KOIs. In addition, we also exclude KOI-981.01 as our attempts to fit the light curve were unable to retrieve a converged, unimodal ephemeris due to excessive correlated noise. This leaves us with 41 KOIs for our survey, which are listed in the first column of Table 1. Note that we include KOIs regardless as to whether they have been dispositioned as a false-positive or not, since the theory of AP is general for any eclipsing body, not just planets (Kipping 2014a).

### 2.2. Detrending & Fitting the Transits

We here describe the procedure used to detrend and fit the *Kepler* transit light curves. We first downloaded all available light curves spanning quarters 1-16 for each object from the Mikulski Archive for Space Telescopes (MAST) database<sup>6</sup>. Where available we use the short-cadence (SC) data over the long-cadence (LC) and we always use the Simple Aperture Photometry (SAP) time series. We exclude all data greater than three transit durations either side of the times of transit minimum.

For each KOI, our goal is to derive posterior distributions for the fitted parameters in a Bayesian framework. This is achieved by coupling a Bayesian regression routine to a transit light curve model. To model

<sup>6</sup> See [http://archive.stsci.edu/kepler/data\\_search/search.php](http://archive.stsci.edu/kepler/data_search/search.php)

the transits, we make the same idealized assumptions as Seager & Mallen-Orn elas (2003) e.g. spherical planet, spherical star, circular orbits, no blended light, opaque planet, etc. The transit light curves are generated using the Mandel & Agol (2002) algorithm described by seven free parameters with the following priors:

- $\log_{10}(\rho_{\star,\text{obs}} [\text{kg m}^{-3}])$ : log-base-ten of the observed stellar density. Uniform prior from  $0 < \log_{10}(\rho_{\star,\text{obs}} [\text{kg m}^{-3}]) < 6$ .
- $(R_P/R_\star) = p$ : ratio of the planetary candidate’s radius to the star’s radius. Uniform prior  $0 < (R_P/R_\star) < 1$ .
- $b$ : impact parameter of the transit. Uniform prior  $0 < b < 2$ .
- $P$ : orbital period of the planet. Uniform prior  $(\bar{P} - 1 [\text{d}]) < P < (\bar{P} + 1 [\text{d}])$ , where  $\bar{P}$  is the period reported by Borucki et al. (2011).
- $\tau$ : time of transit minimum. Uniform prior  $(\bar{\tau} - 1 [\text{d}]) < \tau < (\bar{\tau} + 1 [\text{d}])$ , where  $\bar{\tau}$  is the period reported by Borucki et al. (2011).
- $q_1$ : First modified quadratic limb darkening coefficient defined in Kipping (2013a). Uniform prior  $0 < q_1 < 1$ .
- $q_2$ : Second modified quadratic limb darkening coefficient defined in Kipping (2013a). Uniform prior  $0 < q_2 < 1$ .

We highlight that the stellar density is fitted uniformly in log-space, which can also be thought of as a Jeffreys prior in  $\rho_{\star,\text{obs}}$  (Jeffreys 1946). We choose a Jeffreys prior for this term since it can span several orders of magnitude and it is generally considered the most uninformative prior choice possible. We also highlight that the limb darkening coefficients use the uninformative priors proposed in Kipping (2013a), which both improves the sampling efficiency and ensures complete coverage of the physically permissible prior volume. Long-cadence data are resampled to account for smearing using  $N_{\text{resam}} = 30$  and the technique described in Kipping (2010).

In general, our Bayesian regression routine is a Markov Chain Monte Carlo (MCMC) algorithm (see Gregory 2005 for the use of MCMC in uncertainty estimates) using the Metropolis-Hastings rule (Metropolis et al. 1953; Hastings 1970). We use a Gaussian likelihood function in all fits and the seven parameters are allowed to vary with jump sizes tuned to be between 10% and 100% of the parameter uncertainties with the goal of  $\simeq 10\%$ -40% of trials accepted. For each trial, we first compute the trial model and then determine the best fitting linear slope for each transit epoch which matches the observations and the trial model. This is achieved using a least squares linear minimization routine at every trial and naturally for cases where there are many transits and SC data, the computational time to achieve this is significant (see Kundurthy et al. 2013 for a previous example of this technique). Nevertheless, this approach essentially detrends the data simultaneously to fitting the actual transit model and thus the parameter uncertainties are more realistic.

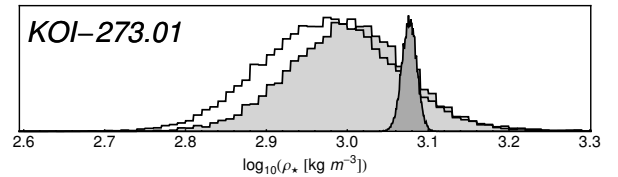


FIG. 1.— Comparison of the posterior distribution for the light curve derived stellar density,  $\rho_{\star,\text{obs}}$ , computed using CoFiAM plus MULTINEST (black outline with white fill) versus linear slope plus MCMC (light gray). Dark gray histogram shows the asteroseismic posterior for reference.

In certain cases, visual inspection of the light curves revealed that linear detrending was insufficient to adequately correct the photometry, since substantial curvature existed in the out-of-transit baseline data. These cases were usually, but not exclusively, long-period KOIs, since such transits have longer transit durations and thus the baseline can cover several days. In these cases, we opted to use a more sophisticated detrending algorithm devised by the Hunt for Exomoons with Kepler (HEK) project (Kipping et al. 2012b) known as CoFiAM (see Kipping et al. 2013 for details). This algorithm is well suited for longer-period planets and works on a Fourier-basis to guarantee that the transit profile remains undisturbed by the detrending procedure. The detrended light curves are then fitted using a multimodal nested algorithm, MULTINEST (Feroz et al. 2008, 2009), rather than MCMC, since MULTINEST is both more expedient in low-dimensional space and requires no tuning of jump sizes.

It is important to note that the regression algorithms are both well-established Bayesian Monte Carlo routines with identical input priors and thus the inferred posterior distributions are statistically equivalent. In cases where linear detrending is sufficient, one should expect consistent results between CoFiAM plus MULTINEST versus linear detrending plus MCMC. This was verified in the example of KOI-273.01, where we infer a nearly-identical a-posteriori distribution for  $\rho_{\star,\text{obs}}$ , as shown in Figure 1.

### 3. RESULTS

#### 3.1. Conducting AP

We provide all of the fitted transit parameters for the 41 KOIs in our sample in Table 1, except for  $\tau$  as this is the least relevant term for our study (available upon request). Table 2 provides a direct comparison of  $\rho_{\star,\text{obs}}$  and  $\rho_{\star,\text{astero}}$ , which is essentially the act of AP (this is also visualized in Figure 2). As discussed in §2.1, any significant AP discrepancies in this sample are likely due to either the PE effect, the PB effect or that the transiting body in fact orbits an alternative star to the asteroseismically measured target. For each of these three possible explanations, we can quantify a relevant descriptive parameter. For the PE effect, the minimum eccentricity,  $e_{\text{min}}$ , naturally falls out of the AP expressions and we use Equation 39 of Kipping (2014a), the results of which are shown in Column 4 of Table 2. Similarly, for the PB effect we use Equation 17 of Kipping (2014a), with results shown in Column 5 of Table 2, provided  $b < (1 - p)$  which is an underlying assumption for the derivation of the PB effect.

If the transiting body orbits a different star in the same aperture, then we know a) the transit is diluted and so

TABLE 1

Fitted Transit Light Curve Parameters for 41 Single KOIs with Asteroseismology. Rows above the horizontal line have  $\log g > 3.7$  and those below have  $\log g \leq 3.7$ .

KOI	$R_P/R_*$	$\log_{10}(\rho_* [\text{kg m}^{-3}])$	$b$	$P$ [days]	$q_1$	$q_2$
1.01	0.1258 <sup>+0.0020</sup> <sub>-0.0015</sub>	3.1853 <sup>+0.0134</sup> <sub>-0.0096</sub>	0.8442 <sup>+0.0025</sup> <sub>-0.0027</sub>	2.4706123 <sup>+0.0000023</sup> <sub>-0.0000024</sub>	0.344 <sup>+0.037</sup> <sub>-0.034</sub>	0.31 <sup>+0.29</sup> <sub>-0.22</sub>
2.01	0.077738 <sup>+0.000012</sup> <sub>-0.000012</sub>	2.44165 <sup>+0.00058</sup> <sub>-0.00058</sub>	0.50033 <sup>+0.00079</sup> <sub>-0.00078</sub>	2.204735409 <sup>+0.000000015</sup> <sub>-0.000000015</sub>	0.2712 <sup>+0.0014</sup> <sub>-0.0014</sub>	0.3366 <sup>+0.0028</sup> <sub>-0.0028</sub>
7.01	0.02505 <sup>+0.00023</sup> <sub>-0.00024</sub>	2.593 <sup>+0.055</sup> <sub>-0.051</sub>	0.351 <sup>+0.087</sup> <sub>-0.142</sub>	3.2136701 <sup>+0.00000065</sup> <sub>-0.00000065</sub>	0.385 <sup>+0.034</sup> <sub>-0.032</sub>	0.333 <sup>+0.046</sup> <sub>-0.043</sub>
64.01	0.03933 <sup>+0.00014</sup> <sub>-0.00013</sub>	2.463 <sup>+0.022</sup> <sub>-0.021</sub>	0.9380 <sup>+0.0033</sup> <sub>-0.0033</sub>	1.95108246 <sup>+0.00000026</sup> <sub>-0.00000026</sub>	0.474 <sup>+0.022</sup> <sub>-0.022</sub>	0.15 <sup>+0.21</sup> <sub>-0.11</sub>
69.01	0.01508 <sup>+0.00012</sup> <sub>-0.00012</sub>	3.160 <sup>+0.051</sup> <sub>-0.051</sub>	0.346 <sup>+0.086</sup> <sub>-0.129</sub>	4.72673879 <sup>+0.00000053</sup> <sub>-0.00000053</sub>	0.358 <sup>+0.025</sup> <sub>-0.023</sub>	0.386 <sup>+0.041</sup> <sub>-0.039</sub>
75.01	0.03979 <sup>+0.00012</sup> <sub>-0.00012</sub>	1.8538 <sup>+0.0105</sup> <sub>-0.0099</sub>	0.6808 <sup>+0.0063</sup> <sub>-0.0068</sub>	105.881608 <sup>+0.000034</sup> <sub>-0.000034</sub>	0.311 <sup>+0.011</sup> <sub>-0.010</sub>	0.559 <sup>+0.041</sup> <sub>-0.040</sub>
87.01	0.0215 <sup>+0.0017</sup> <sub>-0.0012</sub>	3.47 <sup>+0.35</sup> <sub>-0.46</sub>	0.67 <sup>+0.19</sup> <sub>-0.48</sub>	289.86442 <sup>+0.00088</sup> <sub>-0.00087</sub>	0.41 <sup>+0.32</sup> <sub>-0.16</sub>	0.16 <sup>+0.35</sup> <sub>-0.12</sub>
97.01	0.082950 <sup>+0.000084</sup> <sub>-0.000083</sub>	2.3688 <sup>+0.0032</sup> <sub>-0.0033</sub>	0.5574 <sup>+0.0037</sup> <sub>-0.0036</sub>	4.88548901 <sup>+0.00000018</sup> <sub>-0.00000018</sub>	0.3062 <sup>+0.0088</sup> <sub>-0.0085</sub>	0.354 <sup>+0.016</sup> <sub>-0.015</sub>
98.01	0.045650 <sup>+0.00052</sup> <sub>-0.000077</sub>	2.2252 <sup>+0.0080</sup> <sub>-0.0080</sub>	0.5893 <sup>+0.0075</sup> <sub>-0.0075</sub>	6.79012304 <sup>+0.00000060</sup> <sub>-0.00000060</sub>	0.2760 <sup>+0.0093</sup> <sub>-0.0093</sub>	0.350 <sup>+0.025</sup> <sub>-0.025</sub>
107.01	0.01993 <sup>+0.00022</sup> <sub>-0.00022</sub>	2.679 <sup>+0.064</sup> <sub>-0.145</sub>	0.33 <sup>+0.21</sup> <sub>-0.20</sub>	7.2569658 <sup>+0.0000043</sup> <sub>-0.0000043</sub>	0.392 <sup>+0.090</sup> <sub>-0.075</sub>	0.35 <sup>+0.11</sup> <sub>-0.10</sub>
113.01	0.75 <sup>+0.17</sup> <sub>-0.28</sub>	3.703 <sup>+0.048</sup> <sub>-0.067</sub>	1.56 <sup>+0.18</sup> <sub>-0.30</sub>	386.5980986 <sup>+0.0000007</sup> <sub>-0.0000017</sub>	0.609 <sup>+0.089</sup> <sub>-0.083</sub>	0.15 <sup>+0.22</sup> <sub>-0.11</sub>
118.01	0.01549 <sup>+0.00056</sup> <sub>-0.00028</sub>	2.964 <sup>+0.077</sup> <sub>-0.237</sub>	0.34 <sup>+0.28</sup> <sub>-0.26</sub>	24.993233 <sup>+0.000040</sup> <sub>-0.000042</sub>	0.29 <sup>+0.15</sup> <sub>-0.12</sub>	0.44 <sup>+0.31</sup> <sub>-0.25</sub>
122.01	0.02061 <sup>+0.00014</sup> <sub>-0.00019</sub>	3.246 <sup>+0.012</sup> <sub>-0.046</sub>	0.13 <sup>+0.16</sup> <sub>-0.12</sub>	11.5230707 <sup>+0.0000040</sup> <sub>-0.0000040</sub>	0.369 <sup>+0.067</sup> <sub>-0.060</sub>	0.314 <sup>+0.087</sup> <sub>-0.079</sub>
257.01	0.02371 <sup>+0.00050</sup> <sub>-0.00081</sub>	2.985 <sup>+0.031</sup> <sub>-0.031</sub>	0.8621 <sup>+0.0073</sup> <sub>-0.0081</sub>	6.8834063 <sup>+0.0000012</sup> <sub>-0.0000012</sub>	0.298 <sup>+0.023</sup> <sub>-0.023</sub>	0.47 <sup>+0.28</sup> <sub>-0.28</sub>
263.01	0.01466 <sup>+0.00081</sup> <sub>-0.00096</sub>	3.03 <sup>+0.36</sup> <sub>-0.29</sub>	0.70 <sup>+0.12</sup> <sub>-0.042</sub>	20.719416 <sup>+0.000028</sup> <sub>-0.000029</sub>	0.38 <sup>+0.30</sup> <sub>-0.13</sub>	0.29 <sup>+0.41</sup> <sub>-0.22</sub>
268.01	0.02063 <sup>+0.00028</sup> <sub>-0.00015</sub>	2.691 <sup>+0.041</sup> <sub>-0.118</sub>	0.26 <sup>+0.21</sup> <sub>-0.20</sub>	110.37849 <sup>+0.00013</sup> <sub>-0.00013</sub>	0.339 <sup>+0.072</sup> <sub>-0.061</sub>	0.146 <sup>+0.082</sup> <sub>-0.080</sub>
269.01	0.01056 <sup>+0.00036</sup> <sub>-0.00033</sub>	2.05 <sup>+0.23</sup> <sub>-0.22</sub>	0.825 <sup>+0.053</sup> <sub>-0.089</sub>	18.011628 <sup>+0.000030</sup> <sub>-0.000029</sub>	0.375 <sup>+0.067</sup> <sub>-0.059</sub>	0.045 <sup>+0.070</sup> <sub>-0.038</sub>
273.01	0.0214 <sup>+0.0017</sup> <sub>-0.0011</sub>	2.959 <sup>+0.083</sup> <sub>-0.080</sub>	0.9325 <sup>+0.0086</sup> <sub>-0.0100</sub>	10.5737625 <sup>+0.0000072</sup> <sub>-0.0000071</sub>	0.608 <sup>+0.083</sup> <sub>-0.092</sub>	0.49 <sup>+0.34</sup> <sub>-0.32</sub>
276.01	0.01978 <sup>+0.00083</sup> <sub>-0.00074</sub>	3.30 <sup>+0.23</sup> <sub>-0.22</sub>	0.59 <sup>+0.14</sup> <sub>-0.36</sub>	41.746004 <sup>+0.000032</sup> <sub>-0.000032</sub>	0.396 <sup>+0.143</sup> <sub>-0.087</sub>	0.26 <sup>+0.32</sup> <sub>-0.15</sub>
280.01	0.01952 <sup>+0.00045</sup> <sub>-0.00031</sub>	3.036 <sup>+0.074</sup> <sub>-0.060</sub>	0.866 <sup>+0.013</sup> <sub>-0.018</sub>	11.8728958 <sup>+0.000044</sup> <sub>-0.000044</sub>	0.363 <sup>+0.044</sup> <sub>-0.043</sub>	0.18 <sup>+0.24</sup> <sub>-0.14</sub>
281.01	0.01695 <sup>+0.00058</sup> <sub>-0.00069</sub>	2.21 <sup>+0.25</sup> <sub>-0.19</sub>	0.62 <sup>+0.11</sup> <sub>-0.32</sub>	19.556609 <sup>+0.000023</sup> <sub>-0.000023</sub>	0.392 <sup>+0.091</sup> <sub>-0.070</sub>	0.32 <sup>+0.17</sup> <sub>-0.15</sub>
288.01	0.01377 <sup>+0.00035</sup> <sub>-0.00031</sub>	2.40 <sup>+0.14</sup> <sub>-0.14</sub>	0.48 <sup>+0.14</sup> <sub>-0.27</sub>	10.2753113 <sup>+0.000055</sup> <sub>-0.000055</sub>	0.334 <sup>+0.055</sup> <sub>-0.047</sub>	0.40 <sup>+0.12</sup> <sub>-0.10</sub>
319.01	0.0485 <sup>+0.0019</sup> <sub>-0.0019</sub>	2.344 <sup>+0.025</sup> <sub>-0.027</sub>	0.9050 <sup>+0.0041</sup> <sub>-0.0042</sub>	46.151110 <sup>+0.000026</sup> <sub>-0.000026</sub>	0.430 <sup>+0.039</sup> <sub>-0.036</sub>	0.58 <sup>+0.30</sup> <sub>-0.39</sub>
975.01	0.007573 <sup>+0.000019</sup> <sub>-0.000019</sub>	2.7520 <sup>+0.0045</sup> <sub>-0.0061</sub>	0.178 <sup>+0.023</sup> <sub>-0.018</sub>	2.78581687 <sup>+0.0000057</sup> <sub>-0.0000063</sub>	0.280 <sup>+0.029</sup> <sub>-0.029</sub>	0.425 <sup>+0.057</sup> <sub>-0.053</sub>
1282.01	0.04729 <sup>+0.00105</sup> <sub>-0.00072</sub>	2.636 <sup>+0.037</sup> <sub>-0.110</sub>	0.23 <sup>+0.22</sup> <sub>-0.18</sub>	30.863933 <sup>+0.000078</sup> <sub>-0.000080</sub>	0.36 <sup>+0.20</sup> <sub>-0.14</sub>	0.48 <sup>+0.28</sup> <sub>-0.20</sub>
1537.01	0.00720 <sup>+0.00071</sup> <sub>-0.00032</sub>	2.45957 <sup>+0.120555</sup> <sub>-0.383943</sub>	0.43 <sup>+0.32</sup> <sub>-0.29</sub>	10.191592 <sup>+0.000045</sup> <sub>-0.000049</sub>	0.47 <sup>+0.25</sup> <sub>-0.20</sub>	0.66 <sup>+0.25</sup> <sub>-0.31</sub>
1618.01	0.00514 <sup>+0.00014</sup> <sub>-0.00013</sub>	2.734 <sup>+0.046</sup> <sub>-0.147</sub>	0.23 <sup>+0.28</sup> <sub>-0.20</sub>	2.3643709 <sup>+0.000064</sup> <sub>-0.000062</sub>	0.25 <sup>+0.25</sup> <sub>-0.16</sub>	0.25 <sup>+0.43</sup> <sub>-0.20</sub>
1621.01	0.01199 <sup>+0.00048</sup> <sub>-0.00031</sub>	2.998 <sup>+0.080</sup> <sub>-0.080</sub>	0.36 <sup>+0.34</sup> <sub>-0.27</sub>	20.310507 <sup>+0.000053</sup> <sub>-0.000054</sub>	0.27 <sup>+0.29</sup> <sub>-0.15</sub>	0.18 <sup>+0.36</sup> <sub>-0.23</sub>
1890.01	0.00954 <sup>+0.00032</sup> <sub>-0.00014</sub>	2.679 <sup>+0.032</sup> <sub>-0.264</sub>	0.30 <sup>+0.35</sup> <sub>-0.22</sub>	4.3364290 <sup>+0.000034</sup> <sub>-0.000038</sub>	0.38 <sup>+0.15</sup> <sub>-0.11</sub>	0.37 <sup>+0.23</sup> <sub>-0.20</sub>
1924.01	0.004264 <sup>+0.000065</sup> <sub>-0.000056</sub>	1.815 <sup>+0.014</sup> <sub>-0.017</sub>	0.341 <sup>+0.035</sup> <sub>-0.032</sub>	2.1191569 <sup>+0.000023</sup> <sub>-0.000021</sub>	0.986 <sup>+0.010</sup> <sub>-0.013</sub>	0.99955 <sup>+0.00045</sup> <sub>-0.00160</sub>
1962.01	0.03700 <sup>+0.00137</sup> <sub>-0.00092</sub>	4.064 <sup>+0.066</sup> <sub>-0.221</sub>	0.31 <sup>+0.29</sup> <sub>-0.23</sub>	32.858685 <sup>+0.000051</sup> <sub>-0.000055</sub>	0.36 <sup>+0.31</sup> <sub>-0.17</sub>	0.39 <sup>+0.34</sup> <sub>-0.26</sub>
371.01	0.40 <sup>+0.45</sup> <sub>-0.29</sub>	2.85 <sup>+0.14</sup> <sub>-0.12</sub>	1.36 <sup>+0.45</sup> <sub>-0.30</sub>	498.3915 <sup>+0.0012</sup> <sub>-0.0012</sub>	0.33 <sup>+0.30</sup> <sub>-0.25</sub>	0.66 <sup>+0.25</sup> <sub>-0.37</sub>
674.01	0.03772 <sup>+0.00029</sup> <sub>-0.00020</sub>	2.274 <sup>+0.013</sup> <sub>-0.038</sub>	0.15 <sup>+0.13</sup> <sub>-0.11</sub>	16.338893 <sup>+0.000013</sup> <sub>-0.000013</sub>	0.356 <sup>+0.062</sup> <sub>-0.055</sub>	0.511 <sup>+0.092</sup> <sub>-0.079</sub>
1222.01	0.00513 <sup>+0.00049</sup> <sub>-0.00035</sub>	2.74 <sup>+0.15</sup> <sub>-0.41</sub>	0.41 <sup>+0.35</sup> <sub>-0.28</sub>	4.285768 <sup>+0.000013</sup> <sub>-0.000061</sub>	0.54 <sup>+0.32</sup> <sub>-0.34</sub>	0.53 <sup>+0.35</sup> <sub>-0.35</sub>
1230.01	0.07859 <sup>+0.00019</sup> <sub>-0.00020</sub>	1.9996 <sup>+0.0086</sup> <sub>-0.0082</sub>	0.317 <sup>+0.019</sup> <sub>-0.021</sub>	165.739391 <sup>+0.000080</sup> <sub>-0.000084</sub>	0.390 <sup>+0.019</sup> <sub>-0.017</sub>	0.441 <sup>+0.021</sup> <sub>-0.021</sub>
1299.01	0.02855 <sup>+0.00057</sup> <sub>-0.00028</sub>	2.118 <sup>+0.044</sup> <sub>-0.084</sub>	0.28 <sup>+0.16</sup> <sub>-0.17</sub>	52.500934 <sup>+0.000048</sup> <sub>-0.000049</sub>	0.287 <sup>+0.036</sup> <sub>-0.033</sub>	0.744 <sup>+0.095</sup> <sub>-0.083</sub>
1314.01	0.01180 <sup>+0.00068</sup> <sub>-0.00031</sub>	1.965 <sup>+0.093</sup> <sub>-0.291</sub>	0.38 <sup>+0.30</sup> <sub>-0.29</sub>	8.575116 <sup>+0.000030</sup> <sub>-0.000031</sub>	0.54 <sup>+0.26</sup> <sub>-0.20</sub>	0.32 <sup>+0.28</sup> <sub>-0.19</sub>
1894.01	0.01739 <sup>+0.00087</sup> <sub>-0.00039</sub>	1.79 <sup>+0.10</sup> <sub>-0.23</sub>	0.41 <sup>+0.25</sup> <sub>-0.31</sub>	5.2879067 <sup>+0.000085</sup> <sub>-0.000085</sub>	0.361 <sup>+0.115</sup> <sub>-0.092</sub>	0.51 <sup>+0.21</sup> <sub>-0.15</sub>
2133.01	0.019429 <sup>+0.000109</sup> <sub>-0.000066</sub>	1.6382 <sup>+0.0066</sup> <sub>-0.0348</sub>	0.093 <sup>+0.160</sup> <sub>-0.093</sub>	6.2467332 <sup>+0.000023</sup> <sub>-0.000046</sub>	0.977 <sup>+0.022</sup> <sub>-0.044</sub>	0.044 <sup>+0.019</sup> <sub>-0.025</sub>
2481.01	0.01460 <sup>+0.00092</sup> <sub>-0.00050</sub>	1.70 <sup>+0.11</sup> <sub>-0.31</sub>	0.39 <sup>+0.30</sup> <sub>-0.27</sub>	33.84513 <sup>+0.00086</sup> <sub>-0.00052</sub>	0.24 <sup>+0.25</sup> <sub>-0.11</sub>	0.85 <sup>+0.11</sup> <sub>-0.24</sub>
2640.01	0.01619 <sup>+0.00064</sup> <sub>-0.00043</sub>	2.33 <sup>+0.16</sup> <sub>-0.43</sub>	0.49 <sup>+0.29</sup> <sub>-0.37</sub>	33.17354 <sup>+0.00014</sup> <sub>-0.00014</sub>	0.104 <sup>+0.118</sup> <sub>-0.072</sub>	0.52 <sup>+0.33</sup> <sub>-0.33</sub>

the photo-blend effect is occurring b) we do not know the “true” stellar density. However, in the case of the photo-blend effect, Kipping (2014a) showed that the observed density can only be altered up to a minimum limit defined as (Equation 13 of Kipping 2014a):

$$\rho_{\star,\text{alt,max}} = \rho_{\star,\text{obs}} \left( \frac{2p_{\text{obs}}(1 + \sqrt{1 - b_{\text{obs}}^2})}{(1 + p_{\text{obs}})^2 - b_{\text{obs}}^2} \right)^{-3/2} \quad (2)$$

Equation 2 reveals the maximum allowed density of the alternative star. Since it is only an upper limit, only cases where  $\rho_{\star,\text{alt,max}}$  is very low allow us to exclude this scenario. We calculate this term for every KOI in Column 6 of Table 2. In the last column, we provide a plausible list of which of these three effects, or no effect at all (“N”), can explain the observation. Note that objects for which  $B < 1$  (where  $B$  is the blend factor defined in Kipping 2014a) correspond to an anti-blend, which could be the consequence of the PS effect (Kipping 2014a). Nevertheless, the PS effect is expected to cause AP deviations

$$\left( \frac{\rho_{\star,\text{obs}}}{\rho_{\star,\text{true}}} \right) \geq \left( \frac{2p_{\text{obs}}(1 + \sqrt{1 - b_{\text{obs}}^2})}{(1 + p_{\text{obs}})^2 - b_{\text{obs}}^2} \right)^{3/2}, \quad (1)$$

where  $p_{\text{obs}}$  and  $b_{\text{obs}}$  are the observed ratio-of-radii and impact parameter, respectively. In the case where  $\rho_{\star,\text{true}}$  is unknown then, we can re-write this as

$\lesssim 10\%$  and thus generally does not have a significant impact. Additionally, although the photo-eccentric effect can explain a diverse range of AP observations, some cases can be rejected as being due to eccentricity if the periastron passage goes inside the star. We define and compute this using:

$$\begin{aligned} (r_{\text{peri}}/R_{\star}) &\leq (a/R_{\star})(1 - e_{\text{min}}), \\ &\leq \left( \frac{\rho_{\star, \text{astero}} GP^2}{3\pi} \right)^{1/3} (1 - e_{\text{min}}). \end{aligned} \quad (3)$$

### 3.2. Ensemble Results

As evident in Table 2, our AP survey of 41 single KOIs reveals numerous strong discrepancies between  $\rho_{\star, \text{obs}}$  and  $\rho_{\star, \text{astero}}$ . By plotting the observed discrepancies as a function of  $\log g$  (values taken from Huber et al. 2013), one immediately identifies an apparent split in the distribution at the boundary of  $\log g = 3.7$  (see Figure 3). We choose  $\log g = 3.7$  as our split since this is a reasonable proxy for the boundary between dwarfs and giants/sub-giants, plus all of the observed densities below this limit have an overestimated value. Performing an Anderson & Darling (1952) test between these two populations reveals a 0.009% chance they are drawn from the same underlying distribution.

The evidence for a significant divide is supported by further analysis too. We decided to investigate how well our measured ( $\rho_{\star, \text{obs}}/\rho_{\star, \text{astero}}$ ) distribution matches that which would be expected if the photo-eccentric effect alone was responsible for the observations. The motivation for this is that the photo-eccentric effect is capable of explaining the greatest range of measurements (Kipping 2014a). We therefore generated a synthetic population of ( $\rho_{\star, \text{obs}}/\rho_{\star, \text{astero}}$ ) measurements using:

$$\left( \frac{\rho_{\star, \text{obs}}}{\rho_{\star, \text{true}}} \right) = \frac{(1 + e \sin \omega)^3}{(1 - e^2)^{3/2}}. \quad (4)$$

Using the code `ECCSAMPLES` (Kipping 2014b), we draw random  $e$  and  $\omega$  samples from the joint probability distribution  $P(e, \omega | \text{object known to transit})$  to generate our synthetic photo-eccentric population. `ECCSAMPLES` assumes a Beta distribution for the underlying probability distribution of  $e$ ,  $P(e)$  with shape parameters  $a$  and  $b$ . In our simulation, we adopt  $a = 0.867$  and  $b = 3.03$ , which has been shown to provide an excellent match to the observed eccentricity distribution from radial velocity surveys (Kipping 2013b). The final synthetic ( $\rho_{\star, \text{obs}}/\rho_{\star, \text{astero}}$ ) distribution is shown in Figure 4 as a gray histogram. Overlaying the observed distributions for the dwarfs and giants immediately demonstrates how different the two samples are. The dwarf sample is fully compatible with the photo-eccentric effect, with a A-D test giving a  $p$ -value of 77.1%. In contrast, the giants are grossly incompatible with the photo-eccentric effect, with a A-D  $p$ -value of 0.003%, or  $4.2\sigma$ .

In considering this puzzling observation, we devised four possible hypotheses which could reconcile this split:

1. The larger pulsations of the giants induce significant time-correlated noise in the folded light curve,

which subsequently skews the  $\rho_{\star, \text{obs}}$  determination.

2. The asteroseismically determined densities systematically underestimate the stellar density for giant stars.
3. Companions to giant stars are highly eccentric and have a dramatically different eccentricity distribution than dwarf stars.
4. A large fraction of the KOIs associated with giant stars in fact orbit a different star within the aperture - cases we define as false-positives.

Hypothesis 1 can be tested by first quantifying the degree of time-correlated noise in the data. The timescale of this spurious noise must have dominant power at  $\nu_{\text{max}}$ , the frequency of maximum asteroseismology power. For many of the targets, Huber et al. (2013) directly provide  $\nu_{\text{max}}$  and where unavailable we use Equation 10 of Kjeldsen & Bedding (1995). We then tried cross-correlating the ( $\rho_{\star, \text{obs}}/\rho_{\star, \text{astero}}$ ) measurements to the transit duration normalized by this timescale. Performing an A-D test about the median of this new variable, as we did with  $\log g$  before, finds no significant split with a  $p$ -value of 3%. We also repeated this exercise using transit depth normalized by the amplitude of the maximum pulsation (computed using Equation 8 of Kjeldsen & Bedding 1995) and this yields a  $p$ -value of 14%. If time-correlated noise was genuinely responsible, one should expect these  $p$ -values should be lower than that found when using  $\log g$  as the variable. Finally, we note that the median period of the giant sample is 25 d and thus the number of transits stacked together is typically large. This folding effect reduces the effect of time-correlated noise as  $N_{\text{transits}}^{-1/2}$  (Pont et al. 2006), further detracting from hypothesis 1. We therefore conclude hypothesis 1 is an improbable explanation for the observed distribution.

Hypothesis 2 seems improbable on the basis that giant stars yield the largest pulsations amplitudes and timescales. Further, the density of the star is typically the most precisely determined parameter from asteroseismology, directly related to the frequency splitting,  $\Delta\nu$  via (Ulrich 1986):

$$\Delta\nu = \frac{(M_{\star}/M_{\odot})^{1/2}}{(R_{\star}/R_{\odot})^{3/2}} \Delta\nu_{\odot}. \quad (5)$$

The possibility that companions to giant stars are highly eccentric, hypothesis 3, has no direct physical motivation. The median *minimum* eccentricity required to explain this observation is 0.60. This appears inconsistent with the planets detected  $\log g \leq 3.7$  stars from radial velocities, for which the median eccentricity is much lower at 0.129 (see [www.exoplanets.org](http://www.exoplanets.org) Wright et al. 2011). Secondly, even though the photo-eccentric effect is expected to yield a small overestimate bias (Kipping 2014a), the fact that none of the objects have an underestimation effect is improbable. Finally, four of the ten giants (KOI-1222.01, KOI-2133.01, KOI-2481.01 & KOI-2640.01) cannot possibly be explained by the photo-eccentric effect, since this requires a periastron passage

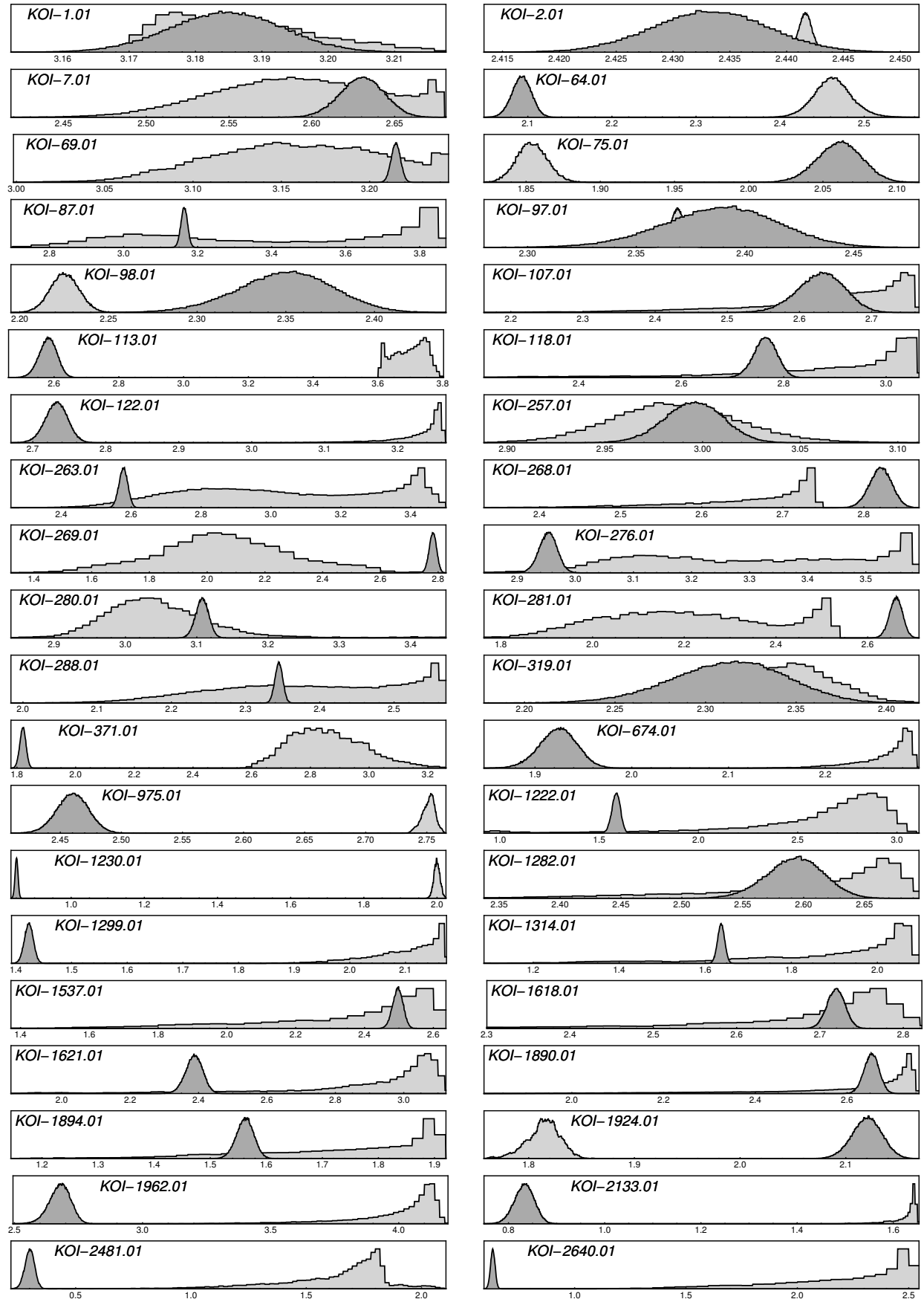


FIG. 2.— Observed (light gray) versus asteroseismically determined (dark gray) mean stellar density posterior distributions for the KOIs in our sample. The x-axis denotes  $\log_{10}(\rho_*$  [ $\text{kg m}^{-3}$ ]). KOI-273.01 is not included but shown in Figure 1.

TABLE 2

Asterodensity profiling parameters for the 41 KOIs in our sample.  $\rho_{\star, \text{astero}}$  values come from Huber et al. (2013). Columns 4, 5 and 6 are computed using Equations 39 & 17 of Kipping (2014a) and Equation 2 of this work, respectively. Classification denotes AP which can explain the observations, where “N” denotes no AP effect required. KOIs with a \* imply that  $b > (1 - p)$  in more than half the posterior samples, meaning the AP equations become invalid. Rows above the horizontal line have  $\log g > 3.7$  and those below have  $\log g \leq 3.7$ .

KOI	$\rho_{\star, \text{obs}}$ [kg m <sup>-3</sup> ]	$\rho_{\star, \text{astero}}$ [kg m <sup>-3</sup> ]	$e_{\text{min}}$	$B$	$\rho_{\star, \text{alt, max}}$ [kg m <sup>-3</sup> ]	Classification
1.01	1532 <sup>+48</sup> <sub>-34</sub>	1530 ± 30	0.0074 <sup>+0.0081</sup> <sub>-0.0051</sub>	0.991 <sup>+0.086</sup> <sub>-0.087</sub>	2636 <sup>+72</sup> <sub>-55</sub>	N
2.01	276.47 <sup>+0.37</sup> <sub>-0.37</sub>	271.2 ± 3.2	0.0064 <sup>+0.0040</sup> <sub>-0.0038</sub>	0.969 <sup>+0.019</sup> <sub>-0.019</sub>	1539.1 <sup>+3.7</sup> <sub>-3.8</sub>	N
7.01	392 <sup>+53</sup> <sub>-43</sub>	427 ± 13	0.034 <sup>+0.036</sup> <sub>-0.023</sub>	1.13 <sup>+0.21</sup> <sub>-0.19</sub>	11600 <sup>+3000</sup> <sub>-2200</sub>	N
64.01	290 <sup>+15</sup> <sub>-14</sub>	123.8 ± 3.3	0.277 <sup>+0.018</sup> <sub>-0.017</sub>	0.192 <sup>+0.017</sup> <sub>-0.016</sub>	753 <sup>+58</sup> <sub>-55</sub>	PE/FP
69.01	1440 <sup>+180</sup> <sub>-160</sub>	1640 ± 10	0.042 <sup>+0.039</sup> <sub>-0.030</sub>	1.19 <sup>+0.21</sup> <sub>-0.18</sub>	89000 <sup>+22000</sup> <sub>-17000</sub>	N
75.01	71.4 <sup>+1.7</sup> <sub>-1.6</sub>	115.2 ± 4.0	0.158 <sup>+0.014</sup> <sub>-0.014</sub>	2.13 <sup>+0.16</sup> <sub>-0.15</sub>	678 <sup>+31</sup> <sub>-28</sub>	FP/PE
87.01	2900 <sup>+3600</sup> <sub>-1900</sub>	1458 ± 30	0.26 <sup>+0.20</sup> <sub>-0.19</sub>	0.37 <sup>+1.42</sup> <sub>-0.24</sub>	66000 <sup>+230000</sup> <sub>-56000</sub>	N
97.01	233.8 <sup>+1.8</sup> <sub>-1.8</sub>	245 ± 15	0.018 <sup>+0.018</sup> <sub>-0.013</sub>	1.08 <sup>+0.12</sup> <sub>-0.11</sub>	1119 <sup>+15</sup> <sub>-15</sub>	N
98.01	168 <sup>+3.2</sup> <sub>-3.1</sub>	224 ± 14	0.096 <sup>+0.021</sup> <sub>-0.022</sub>	1.56 <sup>+0.17</sup> <sub>-0.16</sub>	1614 <sup>+58</sup> <sub>-53</sub>	PB/PE/FP
107.01	478 <sup>+75</sup> <sub>-136</sub>	427 ± 32	0.065 <sup>+0.048</sup> <sub>-0.043</sub>	0.86 <sup>+0.52</sup> <sub>-0.17</sub>	19900 <sup>+6200</sup> <sub>-9100</sub>	N
113.01*	5050 <sup>+580</sup> <sub>-720</sub>	382 ± 24	0.696 <sup>+0.021</sup> <sub>-0.028</sub>	-	-	-
118.01	920 <sup>+180</sup> <sub>-390</sub>	581 ± 30	0.170 <sup>+0.048</sup> <sub>-0.109</sub>	0.53 <sup>+0.60</sup> <sub>-0.12</sub>	55000 <sup>+21000</sup> <sub>-35000</sub>	PE/FP
122.01	1760 <sup>+48</sup> <sub>-177</sub>	540 ± 19	0.372 <sup>+0.015</sup> <sub>-0.029</sub>	0.201 <sup>+0.029</sup> <sub>-0.014</sub>	77700 <sup>+3700</sup> <sub>-13500</sub>	PE/FP
257.01	966 <sup>+76</sup> <sub>-67</sub>	990 ± 34	0.019 <sup>+0.021</sup> <sub>-0.013</sub>	1.04 <sup>+0.14</sup> <sub>-0.13</sub>	8500 <sup>+1300</sup> <sub>-1000</sub>	N
263.01	1070 <sup>+1400</sup> <sub>-520</sub>	378 ± 11	0.33 <sup>+0.22</sup> <sub>-0.21</sub>	0.24 <sup>+0.35</sup> <sub>-0.16</sub>	37000 <sup>+147000</sup> <sub>-26000</sub>	PE/FP
268.01	491 <sup>+49</sup> <sub>-117</sub>	662 ± 21	0.100 <sup>+0.088</sup> <sub>-0.033</sub>	1.53 <sup>+0.73</sup> <sub>-0.20</sub>	20500 <sup>+3900</sup> <sub>-7900</sub>	PB/PE/FP
269.01	113 <sup>+79</sup> <sub>-44</sub>	605 ± 18	0.51 <sup>+0.11</sup> <sub>-0.14</sub>	12.1 <sup>+20.9</sup> <sub>-7.2</sub>	3700 <sup>+6300</sup> <sub>-2200</sub>	FP/PE
273.01	910 <sup>+190</sup> <sub>-150</sub>	1193 ± 25	0.091 <sup>+0.061</sup> <sub>-0.056</sub>	1.65 <sup>+0.81</sup> <sub>-0.50</sub>	4600 <sup>+1700</sup> <sub>-1200</sub>	N
276.01	2010 <sup>+1440</sup> <sub>-790</sub>	898 ± 32	0.26 <sup>+0.056</sup> <sub>-0.16</sub>	0.32 <sup>+0.32</sup> <sub>-0.16</sub>	61000 <sup>+104000</sup> <sub>-37000</sub>	PE/FP
280.01	1090 <sup>+200</sup> <sub>-140</sub>	1281 ± 27	0.059 <sup>+0.045</sup> <sub>-0.039</sub>	1.29 <sup>+0.33</sup> <sub>-0.30</sub>	12200 <sup>+4400</sup> <sub>-2700</sub>	PB/PE/FP
281.01	160 <sup>+124</sup> <sub>-57</sub>	459 ± 15	0.34 <sup>+0.12</sup> <sub>-0.18</sub>	4.6 <sup>+5.1</sup> <sub>-2.6</sub>	5600 <sup>+10600</sup> <sub>-3100</sub>	FP/PE
288.01	249 <sup>+92</sup> <sub>-69</sub>	221.2 ± 2.7	0.081 <sup>+0.068</sup> <sub>-0.057</sub>	0.85 <sup>+0.49</sup> <sub>-0.29</sub>	15100 <sup>+11900</sup> <sub>-6900</sub>	N
319.01	221 <sup>+13</sup> <sub>-13</sub>	206 ± 15	0.027 <sup>+0.028</sup> <sub>-0.010</sub>	0.87 <sup>+0.18</sup> <sub>-0.15</sub>	637 <sup>+50</sup> <sub>-45</sub>	N
975.01	564.9 <sup>+5.8</sup> <sub>-7.9</sub>	288.6 ± 8.7	0.220 <sup>+0.010</sup> <sub>-0.010</sub>	0.405 <sup>+0.018</sup> <sub>-0.017</sub>	105800 <sup>+1900</sup> <sub>-2600</sub>	PE/FP
1282.01	432 <sup>+39</sup> <sub>-97</sub>	392 ± 21	0.048 <sup>+0.034</sup> <sub>-0.031</sub>	0.88 <sup>+0.40</sup> <sub>-0.13</sub>	5750 <sup>+860</sup> <sub>-2110</sub>	N
1537.01	288 <sup>+92</sup> <sub>-169</sub>	314 ± 11	0.078 <sup>+0.235</sup> <sub>-0.053</sub>	1.12 <sup>+2.67</sup> <sub>-0.35</sub>	49000 <sup>+33000</sup> <sub>-41000</sub>	N
1618.01	542 <sup>+60</sup> <sub>-155</sub>	524 ± 13	0.040 <sup>+0.061</sup> <sub>-0.027</sub>	0.96 <sup>+0.55</sup> <sub>-0.13</sub>	179000 <sup>+29000</sup> <sub>-86000</sub>	N
1621.01	1000 <sup>+200</sup> <sub>-530</sub>	244 ± 14	0.436 <sup>+0.051</sup> <sub>-0.182</sub>	0.150 <sup>+0.251</sup> <sub>-0.034</sub>	86000 <sup>+34000</sup> <sub>-65000</sub>	PE/FP
1890.01	478 <sup>+66</sup> <sub>-218</sub>	450 ± 17	0.060 <sup>+0.035</sup> <sub>-0.016</sub>	0.93 <sup>+1.21</sup> <sub>-0.16</sub>	60000 <sup>+16000</sup> <sub>-41000</sub>	N
1924.01	65.3 <sup>+2.2</sup> <sub>-2.5</sub>	131.9 ± 4.3	0.230 <sup>+0.016</sup> <sub>-0.015</sub>	2.58 <sup>+0.18</sup> <sub>-0.16</sub>	25900 <sup>+2000</sup> <sub>-2200</sub>	FP/PE
1962.01	11600 <sup>+1900</sup> <sub>-4600</sub>	477 ± 45	0.785 <sup>+0.023</sup> <sub>-0.073</sub>	0.0126 <sup>+0.0106</sup> <sub>-0.0028</sub>	207000 <sup>+59000</sup> <sub>-124000</sub>	PE/FP
371.01*	710 <sup>+270</sup> <sub>-170</sub>	66.1 ± 1.6	0.658 <sup>+0.057</sup> <sub>-0.054</sub>	-	-	-
674.01	187.8 <sup>+5.6</sup> <sub>-15.7</sub>	84.0 ± 3.7	0.259 <sup>+0.019</sup> <sub>-0.027</sub>	0.325 <sup>+0.041</sup> <sub>-0.026</sub>	3510 <sup>+190</sup> <sub>-520</sub>	PE/FP
1222.01	540 <sup>+270</sup> <sub>-340</sub>	38.5 ± 1.9	0.707 <sup>+0.063</sup> <sub>-0.211</sub>	0.029 <sup>+0.070</sup> <sub>-0.012</sub>	-	FP
1230.01	99.9 <sup>+2.0</sup> <sub>-1.9</sub>	7.091 ± 0.067	0.7073 <sup>+0.0036</sup> <sub>-0.0035</sub>	0.02216 <sup>+0.00057</sup> <sub>-0.00057</sub>	646 <sup>+23</sup> <sub>-22</sub>	PE/FP
1299.01	131 <sup>+14</sup> <sub>-23</sub>	26.50 ± 0.49	0.488 <sup>+0.025</sup> <sub>-0.051</sub>	0.109 <sup>+0.032</sup> <sub>-0.013</sub>	3410 <sup>+700</sup> <sub>-1000</sub>	PE/FP
1314.01	92 <sup>+22</sup> <sub>-45</sub>	42.33 ± 0.82	0.259 <sup>+0.062</sup> <sub>-0.154</sub>	0.345 <sup>+0.510</sup> <sub>-0.086</sub>	7900 <sup>+3900</sup> <sub>-5700</sub>	N
1894.01	62 <sup>+16</sup> <sub>-26</sub>	36.5 ± 1.3	0.180 <sup>+0.069</sup> <sub>-0.123</sub>	0.49 <sup>+0.54</sup> <sub>-0.13</sub>	2900 <sup>+1700</sup> <sub>-1900</sub>	PE/FP
2133.01	43.47 <sup>+0.67</sup> <sub>-3.35</sub>	6.81 ± 0.32	0.547 <sup>+0.013</sup> <sub>-0.019</sub>	0.0813 <sup>+0.0092</sup> <sub>-0.0061</sub>	2113 <sup>+297</sup> <sub>-297</sub>	FP
2481.01	50 <sup>+14</sup> <sub>-26</sub>	1.999 ± 0.096	0.791 <sup>+0.030</sup> <sub>-0.104</sub>	0.0128 <sup>+0.018</sup> <sub>-0.0037</sub>	3200 <sup>+1600</sup> <sub>-2400</sub>	FP
2640.01	212 <sup>+97</sup> <sub>-133</sub>	4.29 ± 0.10	0.862 <sup>+0.029</sup> <sub>-0.113</sub>	0.0051 <sup>+0.0127</sup> <sub>-0.0020</sub>	10200 <sup>+9800</sup> <sub>-8400</sub>	FP

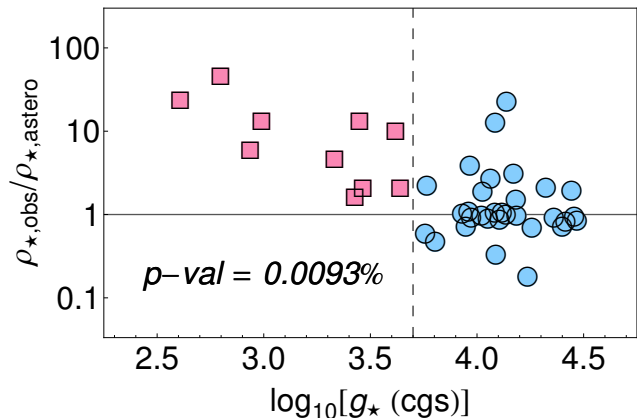


FIG. 3.— Measured ( $\rho_{\star, \text{obs}}/\rho_{\star, \text{astero}}$ ) from this survey (y-axis) as a function of the associated star’s  $\log g$ . Squares correspond to measurements with  $\log g \leq 3.7$  and circles for  $\log g > 3.7$ . The p-value comes from an A-D test between the two populations, showing a significant difference.

inside the star, which we deem unphysical. We therefore find the super-eccentric planets hypothesis strongly disfavored.

By deduction, this leaves us with hypothesis 4 as the only viable explanation. As discussed in §4, this appears consistent with independent arguments regarding the false-positive rate for this sample. Given the small number statistics involved with a sample of just 10 giant star KOIs, the precision to which the associated false-positive rate (FPR) can be measured is naturally low. However, from Figure 4, we estimate that three of the ten giant star KOIs have ( $\rho_{\star, \text{obs}}/\rho_{\star, \text{astero}}$ ) compatible with the synthetic photo-eccentric effect population. The other seven have sufficiently high ( $\rho_{\star, \text{obs}}/\rho_{\star, \text{astero}}$ ) measurements that they appear incompatible with the synthetic photo-eccentric population. On this basis, we estimate  $\text{FPR} \simeq (70 \pm 30)\%$ . We further note that the FPR can easily be seen to be at least  $\text{FPR} \gtrsim (40 \pm 20)\%$ , on the basis that four of the ten KOIs are classified unambiguously as false-positives in Table 2, since they would have to be so eccentric they would pass inside or contact the star.

### 3.3. Kepler-91b: A False-Positive?

Recently, Lillo-Box et al. (2013) claimed to confirm the planetary nature of KOI-2133.01, or Kepler-91b, which is an object in our sample. If this KOI was genuinely a planet, it would seem to be a counter-example to our conclusion of a high false-positive rate for giant host stars. Further, in Table 2 we identify KOI-2133.01 as an unambiguous FP using AP. For these reasons, it is important that we investigate this apparent discrepancy.

The key reason why we identified this object as a false-positive is because  $\rho_{\star, \text{obs}}$  is so much larger than  $\rho_{\star, \text{astero}}$  that the orbit would have to be highly eccentric, such that  $(r_{\text{peri}}/R_{\star}) = 1.10^{+0.06}_{-0.05}$  i.e. the planet is essentially in-contact with the star. Specifically, we have  $\rho_{\star, \text{astero}} = 6.81 \pm 0.032 \text{ kg m}^{-3}$  but  $\rho_{\star, \text{obs}} = 43.47^{+0.67}_{-3.35} \text{ kg m}^{-3}$ , which may be equivalently expressed in terms of the semi-major axis using Kepler’s Third Law as  $(a/R_{\star})_{\text{obs}} = 4.476^{+0.023}_{-0.118}$ . Critically, Lillo-Box et al. (2013) find a much lower observed stellar density, which is more com-

patible with  $\rho_{\star, \text{astero}}$  and thus does not require a highly eccentric planet. They report  $\rho_{\star, \text{obs}} = 7.1^{+0.7}_{-1.9} \text{ kg m}^{-3}$ , which is equivalent to  $(a/R_{\star})_{\text{obs}} = 2.32^{+0.07}_{-0.22}$ .

With two dramatically different light curve determinations of  $\rho_{\star, \text{obs}}$ , or equivalently  $(a/R_{\star})_{\text{obs}}$ , it remains unclear which solution is correct. Fortunately, two additional independent studies have also computed light curve solutions for this object, namely Burke et al. (2013) and Esteves et al. (2013). In the case of Burke et al. (2013), Table 1 reports  $(a/R_{\star}) = 4.346$  (no associated uncertainty reported), which is within  $1.1\sigma$  of our solution but  $> 25\sigma$  discrepant to that of Lillo-Box et al. (2013). In the case of Esteves et al. (2013), the authors report  $(a/R_{\star}) = 4.51^{+0.12}_{-0.26}$ , which is in excellent agreement with our solution ( $< 1\sigma$ ) and inconsistent with that of Lillo-Box et al. (2013) ( $> 8\sigma$ ). We note that Lillo-Box et al. (2013) cite Tenenbaum et al. (2013) as finding  $(a/R_{\star}) = (2.64 \pm 0.23)$ , however this value is not actually listed anywhere is Tenenbaum et al. (2013) and the authors have stated this is not a result from their paper (P. Tenenbaum; 2014 private communication).

Additionally, Esteves et al. (2013) also identified KOI-2133.01 as a false-positive using a completely different technique than us. They reported strong phase variations indicative of reflected light and ellipsoidal variations. However, if  $(a/R_{\star}) \simeq 4.5$ , the amplitude of the variations is so great that KOI-2133.01 must be self-luminous and thus a false-positive. Lillo-Box et al. (2013) remark on this but since their  $(a/R_{\star})$  value is much lower, the phase variations can be explained by reflected light without KOI-2133.01 being self-luminous.

We point out that KOI-2133.01 has a short orbital period (6.25 days) giving us 221 transits which we fitted in this work. In general, one does not expect time-correlated noise to phase up coherently when the transits are folded upon a linear ephemeris (Pont et al. 2006). For this reason, the large number of transits for KOI-2133.01 should lead to red noise being heavily attenuated via  $1/\sqrt{N}$ , where  $N$  is the number of transits. For this reason and the reasons discussed in §3.2, it would be surprising if red noise could be responsible for an erroneous  $(a/R_{\star})$ .

It should therefore be clear that the planetary-nature of KOI-2133.01 hangs primarily as to whether  $(a/R_{\star}) \simeq 4.5$ , in which case it is a false-positive, or  $(a/R_{\star}) \simeq 2.3$ , in which case it can be a planet. With three independent measurements by ourselves, Burke et al. (2013) and Esteves et al. (2013) in agreement versus one study finding the planet scenario (Lillo-Box et al. 2013), the current consensus would favor the false-positive scenario. However, we would encourage multiple independent groups to study this light curve in order to resolve this important question.

## 4. DISCUSSION & CONCLUSIONS

### 4.1. Comparing Our FPR to the Literature

In this work, using the novel technique of AP in isolation, we demonstrate that the false-positive rate of *Kepler* planetary candidates associated with stars of  $\log g \leq 3.7$  (i.e. the giants and sub-giants) is  $\text{FPR} \simeq 70\% \pm 30\%$  (see §3.2). Due to the small-number statistics of our giant-star sample, we prefer the interpretation of a

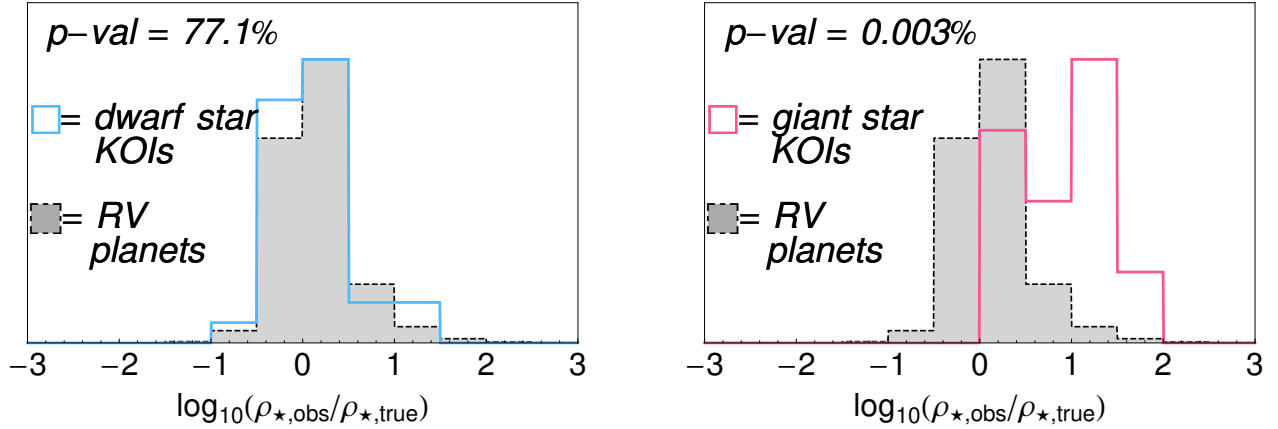


FIG. 4.— Histograms of  $(\rho_{\star,\text{obs}}/\rho_{\star,\text{astro}})$  for KOIs studied in this work. On the left we show the results for those KOIs orbiting dwarf stars ( $\log g > 3.7$ ) and on the right those for giant stars ( $\log g \leq 3.7$ ), demonstrating the clear difference between the two subsets. The gray histogram shows that which would be expected if only the photo-eccentric effect was occurring and the eccentricity distribution matched that observed from the radial velocity planets (Kipping 2013b) deliberately binned to the same scale.

merely “high” false-positive rate, rather than an explicit numerical value. In contrast, we find no compelling evidence for a non-zero FPR of the  $\log g > 3.7$  sample (i.e. the dwarfs). This latter result is consistent with the low FPR for *Kepler* dwarfs reported by Morton & Johnson (2011) and Fressin et al. (2013) of  $\lesssim 10\%$ . However, we are aware of no previous studies characterizing the FPR for *Kepler*’s giant star population.

Although there are no explicit studies regarding *Kepler*’s giant star FPR, numerous other works indicate our result is not a surprise. For example, the population of exoplanets discovered using the radial velocity (RV) technique provides some useful insights. In Figure 5, it is apparent that there is a paucity of planets detected with periods below 100 days for host stars with  $\log g < 3.7$  (1/87), where the data come from [www.exoplanets.org](http://www.exoplanets.org) (Wright et al. 2011). Eight of the ten giant planetary candidates studied in our sample have periods below 100 days though, and therefore seem to occupy a parameter space where radial velocities predict a low occurrence rate. To investigate this further, we estimated the approximate radial velocity amplitudes of the ten KOIs. Approximate masses were estimated from the radii using the empirical relation of Weiss & Marcy (2014) for planets below 4 Earth radii and a simple power-law interpolation through the [www.exoplanets.org](http://www.exoplanets.org) catalog (Wright et al. 2011) for larger worlds, capping masses off at  $1.3 M_J$ . The estimated RV amplitudes are shown as triangles in Figure 5. This reveals that indeed five of the KOIs occupy a region where genuine planets are very rare. This lends credence to the hypothesis that the FPR for our sample is high.

Another useful insight comes from the number of multiple transiting planet systems detected between the dwarfs and giants, since the FPR of multiple planet systems is known to be very low (Lissauer et al. 2012, 2014) at  $\text{FPR} \lesssim 1\%$ . Using the catalog available at <http://exoplanetarchive.ipac.caltech.edu>, we count that 1.8% of host stars with  $\log g \leq 3.7$  and with KOIs not dispositioned as a false-positive reside in multiple transiting KOI systems. In contrast, doing the same for the  $\log g > 3.7$  sample yields 16.9% of the objects. In

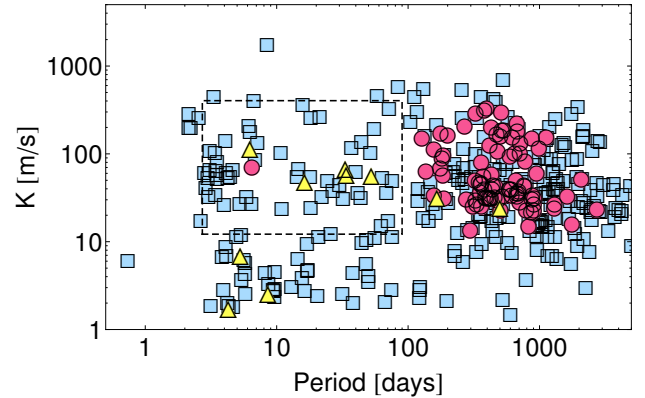


FIG. 5.— Radial velocity semi-amplitudes as a function of the planetary period. Squares denote known planets around host stars with  $\log g > 3.7$  and circles denote those for  $\log g \leq 3.7$ . Triangles represent the estimated position of the giant star KOIs in our sample (not measured radial velocities). The occurrence rate of giant star planets in the dashed box area is very low, with only one known member, HD 102956b (Johnson et al. 2010). The location of five triangles in this region is therefore compatible with a high FPR for giant stars. Data come from [www.exoplanets.org](http://www.exoplanets.org) (Wright et al. 2011).

other words, a *Kepler* star identified to have transiting planetary candidates is nearly 10 times more likely to have multiple candidates if it is a dwarf rather than a giant. This test is not definitive since the number of multi-planet systems orbiting giant stars may genuinely be much lower, but equally it can be explained by an order of magnitude higher false-positive rate for the giants.

We argue that our sample of single KOIs associated with giant stars is largely unbiased, since the only selection criterion is the presence of detectable oscillation modes. This criterion implies that the target a) exhibits large oscillation modes b) is bright enough for these modes to be detected. Amongst the population of giant stars, point a) introduces no significant bias, since the amplitude of maximum oscillation power is enhanced for all low  $\log g$  targets via  $\sim T_{\text{eff}}^2/\log g$  (Kjeldsen & Bedding 1995). The second point implies we

are biased towards brighter targets and so our population may be closer than giant stars without asteroseismic detections. If anything, targets further away may have a higher false-positive rate due to an increased probability of chance alignment. We also note that oscillations may be damped for short-period binaries (Gaulme et al. 2014), however such systems are easily identified via large ellipsoidal variations and beaming effects and unlikely to be a significant source of bias in our sample either.

Our AP survey concludes that many of the giants are false-positives, which specifically is defined as meaning that the transiting body is actually eclipsing a different star. This implies that we should expect many of these KOIs to have potentially detectable companions using adaptive optics (AO) imaging. To investigate this, we use the database of AO images acquired for 715 KOIs by Law et al. (2013). Of these 715, just 19 targets have  $\log g \leq 3.7$  which include the 10 giant star KOIs in our survey ( $\log g$  estimates taken from Huber et al. 2014). Law et al. (2013) report no detections of companions for any of these 19 KOIs, with typical limits of  $\Delta m \simeq 6$  from  $\approx 0''.15$  to  $2''.5$ . However, AO imaging is less constraining for the giants since they are intrinsically brighter and thus in a magnitude-limited survey like *Kepler* will have to be at greater distance from the observer. Using the stellar parameters of Huber et al. (2014), we estimate that the dwarf KOIs ( $\log g > 3.7$ ) have a median distance of  $d = 820^{+420}_{-400}$  pc, whereas the giants ( $\log g \leq 3.7$ ) have  $d = 1500^{+2200}_{-700}$  pc. We therefore do not consider the lack of AO detections to be incompatible with our result.

#### 4.2. Future Possibilities of AP

This work demonstrates the unique power of the relatively new technique of asterodensity profiling. Whilst AP is usually associated with the goal of constraining the orbital eccentricities of exoplanets (Kipping et al. 2012a; Dawson & Johnson 2012), we here verify that the method is also a powerful tool in vetting planetary candidates using photometry alone (Tingley et al. 2011; Kipping 2014a). In this work, we considered just 41 KOIs, but future studies with hundreds or thousands of objects would be able to realistically measure the eccentricity distribution using AP alone. Ensemble studies require targets with homogeneously and accurately derived stellar densities and we encourage work in this area to provide AP a larger sample of targets for future applications.

Future space-based transit survey missions, such as TESS<sup>7</sup> (Ricker et al. 2010) and PLATO (Rauer et al. 2013), will also surely benefit from using AP in both planet validation and characterization and our work highlights the value of accurate stellar parameters for such surveys.

#### ACKNOWLEDGEMENTS

We thank the anonymous reviewer for their helpful comments. We offer our thanks and praise to the extraordinary scientists, engineers and individuals who have made the *Kepler Mission* possible. D. Sliski wishes to thank the Michele and David Mittleman Foundation for their computational support in helping to reduce the mass amount of data. This research has made use of the Exoplanet Orbit Database and the Exoplanet Data Explorer at exoplanets.org.

#### REFERENCES

- Agol, E., Steffen, J., Sari, R. & Clarkson, W., 2005, MNRAS, 359, 567
- Anderson, T. W. & Darling, D. A., 1952, Annals of Mathematical Statistics, 23, 193
- Bastien, F. A., Strassun, K. G., Basri, G. & Pepper, J., 2013, Nature, 500, 427
- Borucki, W. J. et al., 2011, ApJ, 736, 19
- Burke, C. J. et al., 2013, ApJS, 210, 19
- Dawson, R. I. & Johnson, J. A., 2012, ApJ, 756, 122
- Dawson, R. I., Murray-Clay, R. A. & Johnson, J. A., 2013, ApJ, submitted (arXiv:1211.0554)
- Esteves, L. J., de Mooij, E. J. W. & Jayawardhana, R., 2013, ApJ, 772, 51
- Feroz, F. & Hobson, M. P., 2008, MNRAS, 384, 449
- Feroz, F., Hobson, M. P. & Bridges, M., 2009, MNRAS, 398, 1601
- Fressin, F. et al., 2013, ApJ, 766, 81
- Gaulme, P., Jackiewicz, J., Appourchaux, T. & Mosser, B., 2014, ApJ, 785, 5
- Gilliland, R. L. et al., 2010, ApJ, 713, 160
- Gregory P. C., 2005, Bayesian Logical Data Analysis for the Physical Sciences: A Comparative Approach with Mathematica Support. Cambridge University Press
- Hastings, W. H. 1970, Biometrika, 57, 97
- Holman, M. J. & Murray, N. W., 2005, Science, 307, 1288
- Huber, D. et al., 2013, ApJ, 767, 127
- Huber, D. et al., 2014, ApJS, 211, 2
- Jeffreys, H., 1946, Proceedings of the Royal Society of London, Series A, Math. and Phys. Sci. 186, 453
- Johnson, J. A. et al., 2010, ApJ, 721, L153
- Kjeldsen, H. & Bedding, T. R., 1995, A&A, 293, 87
- Kipping, D. M., 2009, MNRAS, 392, 181
- Kipping, D. M., 2010, MNRAS, 408, 1758
- Kipping, D. M., Dunn, W. R., Jasinski, J. M. & Manthri, V. P., 2012a, MNRAS, 421, 1166
- Kipping, D. M., Bakos, G. Á., Buchhave, L. A., Nesvorný, D. & Schmitt, A. 2012b, ApJ, 750, 115
- Kipping, D. M., Hartman, J., Buchhave, L. A., Schmitt, A., Nesvorný, D. & Bakos, G. Á., 2013, ApJ, 770, 101
- Kipping, D. M., 2013a, MNRAS, 435, 2152
- Kipping, D. M., 2013b, MNRAS, 434, L51
- Kipping, D. M., 2014a, MNRAS, 440, 2164
- Kipping, D. M., 2014b, MNRAS, submitted
- Kundurthy, P., Becker, A. C., Agol, E., Barnes, R. & Williams, B., 2013, ApJ, 764, 8
- Law, N. M. et al., 2013, ApJ, submitted (arXiv:1312.4958)
- Lillo-Box, J. et al., 2014, A&A, 562, A109
- Lissauer, J. J. et al., 2012, ApJ, 750, 112
- Lissauer, J. J. et al., 2014, ApJ, 784, 44
- Mandel, K. & Agol, E., 2002, ApJ, 580, 171
- Mazeh, T. et al., 2013, ApJS, 208, 16
- Metropolis, N., Rosenbluth, A. W., Rosenbluth, M. N., Teller, A. H. & Teller, E., 1953, J. Chem. Phys., 21, 1087
- Morton, T. D. & Johnson, J. A., 2011, ApJ, 738, 170
- Nesvorný, D., Kipping, D. M., Buchhave, L. A., Bakos, G. Á., Hartman, J. & Schmitt, A., 2012, Science, 336, 1133
- Nesvorný, D., Kipping, D. M., Terrell, D., Hartman, J., Bakos, G. Á., Buchhave, L. A., 2013, ApJ, 777, 3
- Plavchan, P., Bilinski, C. & Currie, T., 2014, PASP, 126, 34
- Pont, F., Zucker, S. & Queloz, D., 2006, MNRAS, 373, 231
- Rauer, H et al., 2013, Exp. Astron., submitted (astro-ph:1310.0696)

<sup>7</sup> <http://tess.gsfc.nasa.gov/index.html>

- Ricker, G. R. et al., 2010, in *American astronomical society meeting abstracts #215*, vol. 42 of *Bulletin of the American Astronomical Society*, p. 450.06
- Rowe, J. F. et al., 2014, *ApJ*, 784, 45
- Seager, S. & Mallén-Ornelas, G., 2003, *ApJ*, *ApJ*, 585, 1038
- Tenenbaum, P. et al., 2013, *ApJS*, 199, 24
- Tingley, B., Bonomo, A. S. & Deeg, H. J., 2011, *ApJ*, 726, 112
- Torres, G. et al., 2011, *ApJ*, 727, 24
- Ulrich, R. K. 1986, *ApJ*, 306, L37
- Van Eylen, V. et al., 2013, *ApJ*, 782, 14
- Weiss, L. M. & Marcy, G. W., 2014, *ApJ*, 783, L6
- Wright, J. T. et al., 2011, *PASP*, 123, 412